Robust Image Based Visual Servoing with Prescribed Performance under Field of View Constraints

Charalampos P. Bechlioulis, Shahab Heshmati-alamdari, George C. Karras and Kostas J. Kyriakopoulos

***Abstract*—We propose a visual servoing scheme that imposes predefined performance specifications on the image feature coordinate errors and satisfies the visibility constraints that inherently arise owing to the camera's limited field of view, despite the inevitable calibration and depth measurement errors. Its efficiency is demonstrated via a comparative experimental study.**

***Index Terms*—Visual servoing, field of view constraints, robustness.**

I. Introduction

Over the last decades, visual servoing has gained a lot of research interest in motion control systems since it simply employs the visual information of a camera as feedback to determine the required motion control signal. Structurally, visual servoing can be classified in three main categories [1], [2]: (i) Position-Based Visual Servoing (PBVS), where the visual features extracted from the image are used to estimate the $3D$ pose of the camera with respect to the target; (ii) Image-Based Visual Servoing (IBVS), where the control inputs are determined directly on the $2D$ image plane based on the image feature coordinate errors, and (iii) Hybrid Visual Servoing, where $3D$ PBVS is combined with $2D$ IBVS. In this paper, the IBVS scheme is adopted, as it is more efficient and exhibits better local stability and convergence properties, owing to its inherent robustness against camera calibration imperfections and modeling errors.

Since visual servoing is solely based on visual information extracted from the position of the features of interest on the camera image, a significant issue that reasonably raises concerns the satisfaction of certain hard visibility constraints, imposed by the fact that the features of interest should constantly lie within the camera field of view [3]. Although dealing with hard constraints is a rather challenging control task, various methods have been presented in the related literature. More specifically, decoupled control approaches, where the camera motion is controlled in part by a position based scheme, while an image based visual servoing part is employed in order to meet the hard visibility constraints, have been proposed in [4]–[8]. Alternatively, path planning has been applied to develop feasible image feature trajectories that meet the specific field of view constraints in [9]–[11]. Other researchers have adopted optimization techniques that aim at finding an optimal path with respect to various metrics such as the distance from the image boundary, the length of the path and the energy [12]–[14]. Similarly, a nonlinear model predictive control problem is formulated in [15]–[17] to handle the visibility issue via state inequality constraints. However, the aforementioned approaches are based on solving online nonlinear constrained optimization problems; thus, their applicability in real-time robotic tasks is rather questionable, owing to the high processing requirements.

It is also well known that IBVS does not require the geometric model of the target. However, the image Jacobian that is employed involves the intrinsic camera parameters and the depth of the image features with respect to the camera frame. Therefore, accurate camera parameters, which may be acquired via a calibration process, are crucial for the closed loop system performance and stability [18]. Unfortunately, most of the aforementioned approaches adopt off-line calculations to deal with the camera calibration uncertainty, which cannot be performed easily in real-time systems in the presence of 3D model reconstruction errors, thus rendering them impractical. Alternatively, various approaches such as adaptive control [18]–[21], calibration free path planning [11], [22], [23], online identification [24] and machine learning [25] have been proposed in the related literature to achieve the desired stability properties despite any calibration or depth measurement errors. Concurrently, other calibration free solutions have been presented in [10], [11], [26], [27].

Another important issue associated with IBVS concerns the transient and steady state response of the closed loop system[1]. Unfortunately, apart from [26], where bounds on the task error have been addressed, the related literature lacks of any systematic procedure that imposes accurately predefined transient and steady state performance specifications. Towards this direction, the common practice in conventional IBVS under model uncertainties is to tune the control gains via a tedious trial and error procedure without, however, any a priori guarantees for the achieved performance. It should be noted that owing to the presence of multiple and probably conflicting operational constraints (i.e., field of view, transient and steady state specifications, model imperfections) that increase significantly the complexity of the IBVS problem, no results have been previously reported in the related literature, up to the best of the authors' knowledge.

In this work, an IBVS scheme is proposed, capable of guaranteeing prescribed transient and steady state performance as well as the satisfaction of the field of view constraints, despite the inevitable camera calibration and depth measurement errors[2]. Visualizing the performance specifications and the field of view constraints as error bounds, the key idea is to provide an error transformation that converts the original constrained model into an equivalent unconstrained one. It is then proven that stabilizing the unconstrained model is sufficient to achieve prescribed performance guarantees and satisfy the field of view constraints. In particular, the main contributions of this work concentrate on: i) the guaranteed transient and steady state performance; ii) the satisfaction of the field of view constraints and iii) the reduced design complexity. More specifically, the performance of the developed scheme is a priori and explicitly imposed by certain designer-specified performance functions, and is fully decoupled by the control gains selection. In that respect, the selection of the control gains is only confined to adopting those values that lead to reasonable control effort, thus simplifying further the control design. Additionally, the computational complexity of the proposed scheme proves considerably low (i.e., it is a static scheme involving very few and simple calculations to output the control signal), which makes implementation on fast embedded control systems straightforward. Finally, the robustness against the initial pose of the camera is reinforced via the proposed error transformation that retains the image features within the camera field of view. It should be noted that securing merely the boundedness of the closed loop system is sufficient to meet the operational constraints. Such property comes naturally from the appropriate modulation of the feature coordinate errors, which is the key point in our approach. In fact, the size of the set where the modulated errors end up and which is affected by

C. P. Bechlioulis, G. C. Karras and K. J. Kyriakopoulos are with the Control Systems Lab, School of Mechanical Engineering, National Technical University of Athens, 9 Heroon Polytechniou Street, Zografou 15780, Greece. S.Heshmati-alamdari is with the Division of Decision and Control Systems, School of Electrical Engineering and Computer Science, KTH Royal Institute of Technology, Stockholm, Sweden. Emails: {chmpechl,karrasg,kkyria}@mail.ntua.gr, shaha@kth.se. *(Corresponding author: C. P. Bechlioulis.)*

[1]Notice that the ability of preshaping the transient and steady steady response of IBVS is critical in many industrial applications, such as motorized conveyor belt systems or automated loading/unloading processes, where tracking of moving objects is involved.

[2]A preliminary version of this work in the absence of any uncertainties and model imperfections in the closed loop system was reported in [28].

the control gain selection and the uncertainties regarding the camera intrinsic parameters and the depth measurements, does not play a crucial role in the achieved performance. On the other hand, most IBVS schemes examine only convergence within the corresponding stability analysis, while leaving the transient performance (including the field of view constraints) to the "appropriate" (but not a priori guaranteed) control gain selection.

II. Problem Statement

In this section, the mathematical formulation of the image based visual servoing problem is presented for a pinhole camera model. Let $[X_c, Y_c, Z_c]^T$ be the axes of the camera frame $\mathcal{C}$ attached at the center of the camera O_c. The coordinates of the image frame $\mathcal{I}$ are given by $[u, v]^T$ with O_I denoting the center of the image (see Fig.1). Notice that the Z_c axis of the camera frame is perpendicular to the image plane transversing O_I. Thus, given a set of n fixed 3D points

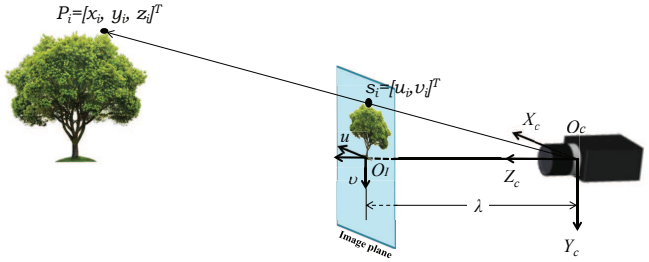

Fig. 1: The geometric model of a pinhole camera.

$P_i = [x_i, y_i, z_i]^T$, $i = 1, \ldots, n$ expressed in the camera frame, the corresponding 2D image features $s_i = [u_i, v_i]^T$, $i = 1, \ldots, n$ are given (in pixels) as follows [1]:

$$s_i = \begin{bmatrix} u_i \\ v_i \end{bmatrix} = \frac{\lambda}{z_i} \begin{bmatrix} x_i \\ y_i \end{bmatrix} \tag{1}$$

where λ is the focal length of the camera. In this way, the effect of the camera motion on the feature coordinates at the image plane is modeled by:

$$\dot{s}_i = L_i(z_i, s_i)V,\ i = 1, \ldots, n \tag{2}$$

where:

$$L_i(z_i,s_i)=\begin{bmatrix} -\frac{\lambda}{z_i} & 0 & \frac{u_i}{z_i} & \frac{u_i v_i}{\lambda} & -\frac{\lambda^2+u_i^2}{\lambda} & v_i \\ 0 & -\frac{\lambda}{z_i} & \frac{v_i}{z_i} & \frac{\lambda^2+v_i^2}{\lambda} & -\frac{u_i v_i}{\lambda} & -u_i \end{bmatrix} \tag{3}$$

is the interaction matrix [1], and $V \triangleq \left[T^T,\ \Omega^T\right] = [T_x, T_y, T_z, \omega_x, \omega_y, \omega_z]^T$ denotes the linear T and angular Ω velocities of the camera. Let us also define the overall image feature vector $s = \left[s_1^T, \cdots, s_n^T\right]^T \in \Re^{2n}$. Hence, the dynamics of the feature coordinates is given by:

$$\dot{s} = L(z, s)V \tag{4}$$

where $L(z, s) = \left[L_1^T(z_1, s_1), \cdots, L_n^T(z_n, s_n)\right]^T \in \Re^{2n\times 6}$ is the overall interaction matrix and $z = [z_1, \ldots, z_n]^T$. Owing to the limited field of view of the camera, the image coordinates are subject to the following visibility constraints:

$$u_{\min} \leq u_i \leq u_{\max},\ i = 1, \ldots, n \tag{5a}$$
$$v_{\min} \leq v_i \leq v_{\max},\ i = 1, \ldots, n \tag{5b}$$

where $u_{\min}$, $v_{\min}$ and $u_{\max}$, $v_{\max}$ denote the lower and upper bounds (in pixels) of the image plane coordinates, dictated by the camera resolution. Ensuring that the feature coordinates do not violate the aforementioned visibility constraints and therefore they constantly lie within the camera field of view is an issue of paramount importance in visual servoing, since otherwise unpredictable phenomena (even instability) may occur in the closed loop system owing to the partial or complete loss of visual feedback.

In this work, the control objective is to design an image based visual servoing scheme such that all feature coordinates $s_i = [u_i, v_i]^T$, $i = 1, \ldots, n$ converge to their corresponding desired values $s_i^d = [u_i^d, v_i^d]^T$, $i = 1, \ldots, n$ with prescribed performance, despite the inevitable camera calibration and depth measurement errors (i.e., the focal length λ and the features depth z_i, $i = 1, \ldots, n$ are not accurately computed). By prescribed performance, we mean that the desired feature coordinates s_i^d, $i = 1, \ldots, n$ are attained within a predefined transient period and are maintained with arbitrarily fine accuracy, while satisfying the field of view constraints (5a) and (5b) for all time.

III. Main Results

In this work, the prescribed performance control technique [29], will be adopted to: i) achieve robust predefined transient as well as steady state response for all image feature errors and ii) avoid the violation of the camera field of view constraints.

A. Sufficient Conditions

Let us initially define the image feature errors:

$$e_i^u(t) = u_i(t) - u_i^d,\ i = 1, \ldots, n \tag{6a}$$
$$e_i^v(t) = v_i(t) - v_i^d,\ i = 1, \ldots, n \tag{6b}$$

where u_i^d, v_i^d denote the corresponding desired feature values, as well as the overall error vector $e \triangleq [e_1^u, e_1^v, \ldots, e_n^u, e_n^v]^T$. Prescribed performance characterizes the behavior when the image feature errors $e_i^u(t)$, $e_i^v(t)$, $i = 1, \ldots, n$ evolve strictly within predefined regions that are bounded by absolutely decaying functions of time, called performance functions. In this work, the mathematical expression of prescribed performance is formulated, for all $t \geq 0$, by the following inequalities:

$$-\underline{M}_i^u \rho_i^u(t) < e_i^u(t) < \bar{M}_i^u \rho_i^u(t),\ i = 1, \ldots, n \tag{7a}$$
$$-\underline{M}_i^v \rho_i^v(t) < e_i^v(t) < \bar{M}_i^v \rho_i^v(t),\ i = 1, \ldots, n \tag{7b}$$

where

$$\rho_i^u(t) = \left(1 - \frac{\rho_\infty}{\max\left\{\underline{M}_i^u, \bar{M}_i^u\right\}}\right)\exp(-lt) + \frac{\rho_\infty}{\max\left\{\underline{M}_i^u, \bar{M}_i^u\right\}} \tag{8a}$$
$$\rho_i^v(t) = \left(1 - \frac{\rho_\infty}{\max\left\{\underline{M}_i^v, \bar{M}_i^v\right\}}\right)\exp(-lt) + \frac{\rho_\infty}{\max\left\{\underline{M}_i^v, \bar{M}_i^v\right\}} \tag{8b}$$

are designer-specified smooth, bounded and decreasing functions of time with l, $\rho_\infty > 0$ incorporating the desired transient and steady state performance specifications respectively, and $\underline{M}_i^u$, $\bar{M}_i^u$, $\underline{M}_i^v$, $\bar{M}_i^v$ are positive parameters selected appropriately to satisfy the field of view constraints, as presented in the sequel. In particular, the decreasing rate of $\rho_i^u(t)$, $\rho_i^v(t)$, which is affected by the parameter l, introduces a lower bound on the speed of convergence of $e_i^u(t)$, $e_i^v(t)$, $i = 1, \ldots, n$. Furthermore, depending on the resolution of the camera, the constant ρ_∞ can be set arbitrarily small $\rho_\infty << \min_{i=1,\ldots,n}\left\{\underline{M}_i^u,\ \bar{M}_i^u,\ \underline{M}_i^v,\ \bar{M}_i^v\right\}$, thus achieving practical convergence of $e_i^u(t)$, $e_i^v(t)$, $i = 1, \ldots, n$ to zero. Additionally, we select:

$$\underline{M}_i^u = u_i^d - u_{\min}\ \&\ \bar{M}_i^u = u_{\max} - u_i^d,\ i = 1, \ldots, n \tag{9a}$$
$$\underline{M}_i^v = v_i^d - v_{\min}\ \&\ \bar{M}_i^v = v_{\max} - v_i^d,\ i = 1, \ldots, n \tag{9b}$$

Apparently, under the assumption that the features initially lie in the camera field of view (i.e., $u_{\min} < u_i(0) < u_{\max}$ and $v_{\min} < v_i(0) < v_{\max}$, $i = 1, \ldots, n$) the aforementioned selection ensures that:

$$-\underline{M}_i^u \rho_i^u(0) < e_i^u(0) < \bar{M}_i^u \rho_i^u(0),\ i = 1, \ldots, n \tag{10a}$$
$$-\underline{M}_i^v \rho_i^v(0) < e_i^v(0) < \bar{M}_i^v \rho_i^v(0),\ i = 1, \ldots, n \tag{10b}$$

Hence, guaranteeing prescribed performance via (7a) and (7b) for all $t > 0$ and employing the decreasing property of $\rho_i^u(t),\ \rho_i^v(t)$, $i = 1, \ldots, n$, we obtain:

$$-\underline{M}_i^u < e_i^u(t) < \bar{M}_i^u,\ i = 1, \ldots, n \tag{11a}$$
$$-\underline{M}_i^v < e_i^v(t) < \bar{M}_i^v,\ i = 1, \ldots, n \tag{11b}$$

and consequently owing to (6a)-(6b) and (9a)-(9b):

$$u_{\min} < u_i(t) < u_{\max}, i = 1, \ldots, n \tag{12a}$$
$$v_{\min} < v_i(t) < v_{\max}, i = 1, \ldots, n \tag{12b}$$

for all $t > 0$, which ensures that the field of view constraints are constantly satisfied. Therefore, imposing prescribed performance via (7a) and (7b) with appropriately selected performance functions $\rho_i^u(t),\ \rho_i^v(t),\ i = 1, \ldots, n$ and positive constant parameters $\underline{M}_i^u,\ \bar{M}_i^u,\ \underline{M}_i^v,\ \bar{M}_i^v,\ i = 1, \ldots, n$, as dictated in (9a) and (9b) respectively, prove sufficient to solve the image based visual servoing problem stated in Section II.

B. Control Design

In the sequel, we propose a control protocol that incorporates neither accurate depth measurements nor accurate focal length estimation, and guarantees (7a) and (7b) for all $t \geq 0$, thus leading to the solution of the robust image based visual servoing problem with prescribed performance under field of view constraints. Given the image feature tracking errors $e_i^u(t)$, $e_i^v(t)$, $i = 1, \ldots, n$, defined in (6a) and (6b), we select the corresponding performance functions $\rho_i^u(t),\ \rho_i^v(t)$ and positive parameters $\underline{M}_i^u,\ \bar{M}_i^u,\ \underline{M}_i^v,\ \bar{M}_i^v, i = 1, \ldots, n$ following (9a) and (9b) respectively, in order to incorporate the desired transient and steady state performance specifications as well as the field of view constraints. We define the normalized image feature errors as:

$$\xi_i^u(u_i, t) = \frac{e_i^u}{\rho_i^u(t)} \quad \& \quad \xi_i^v(v_i, t) = \frac{e_i^v}{\rho_i^v(t)},\ i = 1, \ldots, n$$

and the transformed image feature errors as:

$$E_i^u\left(\xi_i^u(u_i,t)\right) = \ln\left(\frac{1+\frac{\xi_i^u(u_i,t)}{\underline{M}_i^u}}{1-\frac{\xi_i^u(u_i,t)}{\bar{M}_i^u}}\right) \quad \& \quad E_i^v\left(\xi_i^v(v_i,t)\right) = \ln\left(\frac{1+\frac{\xi_i^v(v_i,t)}{\underline{M}_i^v}}{1-\frac{\xi_i^v(v_i,t)}{\bar{M}_i^v}}\right)$$

for which $e_i^u \to 0$ ($e_i^v \to 0$) implies $E_i^u \to 0$ ($E_i^v \to 0$), $i = 1, \ldots, n$. Finally, we design the image based visual servoing protocol as follows:

$$V(s,t) = -k\hat{L}^+ E(s,t) \tag{13}$$

with $k > 0$ where $\hat{L}^+ \triangleq \left(\hat{L}^T\hat{L}\right)^{-1}\hat{L}^T$ is the Moore-Penrose pseudo-inverse of the estimated interaction matrix [23] and

$$E(s,t) \triangleq \left[E_1^u, E_1^v, \ldots, E_n^u, E_n^v\right]^T. \tag{14}$$

Remark 1. *The prescribed performance control technique enforces the normalized image feature errors $\xi_i^u(t)$ and $\xi_i^v(t)$ to remain strictly within the sets $\left(-\underline{M}_i^u,\ \bar{M}_i^u\right)$ and $\left(-\underline{M}_i^v,\ \bar{M}_i^v\right)$, $i = 1, \ldots, n$ respectively for all $t > 0$. Notice that modulating $\xi_i^u(t)$ and $\xi_i^v(t)$ via the logarithmic functions $\ln\left(\frac{1+\frac{\star}{\underline{M}_i^u}}{1-\frac{\star}{\bar{M}_i^u}}\right)$ and $\ln\left(\frac{1+\frac{\star}{\underline{M}_i^v}}{1-\frac{\star}{\bar{M}_i^v}}\right)$ in the control protocol (13) and selecting $\underline{M}_i^u,\ \bar{M}_i^u,\ \underline{M}_i^v,\ \bar{M}_i^v$ according to (9a) and (9b), the overall transformed image feature error vector (14) is initially well-defined. Moreover, it is not difficult to verify that maintaining simply the boundedness of the modulated errors $E_i^u(u_i,t)$ and $E_i^v(v_i,t)$ for all $t > 0$ is equivalent to guaranteeing $\xi_i^u(u_i,t) \in \left(-\underline{M}_i^u,\ \bar{M}_i^u\right)$ and $\xi_i^v(v_i,t) \in \left(-\underline{M}_i^v,\ \bar{M}_i^v\right)$, $i = 1, \ldots, n$ for all $t > 0$. Therefore, the problem at hand can be simply visualized as stabilizing the modulated error vector $E(s,t)$.*

Remark 2. *Regarding the construction of the performance functions, we stress that unlike what is common practice in the related literature, the desired performance specifications concerning the transient and steady state response as well as the field of view constraints are introduced directly in the proposed control scheme via $\rho_i^u(t),\ \rho_i^v(t)$ and the positive parameters $\underline{M}_i^u,\ \bar{M}_i^u,\ \underline{M}_i^v,\ \bar{M}_i^v,\ i = 1, \ldots, n$ respectively. In this way, the selection of the control gain k, that has been isolated from the actual control performance, is significantly simplified to adopting those values that lead to reasonable control effort. Additionally, the proposed method can also take into account holonomic constraints on the camera motion in the Cartesian space by introducing a high level planner that adjusts appropriately the performance bounds. In that respect, the convergence rate of the performance functions may be updated online, and not kept constant, so that certain motion-profiles of the camera in the Cartesian space may be achieved. Notice that since the camera is assumed fully actuated then no controllability issues arise when adjusting the performance bounds. Finally, it is worth noting that the proposed approach achieves tracking of moving features as well, without requesting their velocity profile, as dictated in [30].*

Remark 3. *Notice from (3) that L depends on the depth distribution z of the image features as well as on the camera focal length λ. Thus, considering camera calibration and depth measurement errors, the matrix $\hat{L}$, which is employed in the control design, is an estimate of the actual interaction matrix $L(z,s)$. Under the assumption that L is full column-rank, which is rather realistic in the context of visual servoing, the task function parametrization approach, which aims at providing a controllable system over the task workspace, employs the estimated interaction matrix $\hat{L}$ that is also full column-rank for reasonable focal length and depth estimates. A common approach is to employ the depth distribution at the desired pose with a rough estimate of the focal length via an initial calibration procedure. Alternatively, an estimate of the depth could be adopted following the approach in [21].*

Remark 4. *Under the assumption that the interaction matrix is full column-rank, which holds locally for sufficiently many features [1], this work reinforces the robustness of IBVS against the initial pose of the camera, via the proposed error transformation that retains the image features within the camera field of view. In this respect, the actual/practical domain of attraction is satisfactorily retained in the presence of model uncertainties, as the image features never escape the camera field of view*[3].

C. Stability Analysis

The main results of this work are summarized in the following theorem, where it is proven that the aforementioned control protocol solves the image based visual servoing problem with prescribed performance under field of view constraints, despite the inevitable camera calibration and depth measurement errors.

[3]In the absence of uncertainty in the focal length and the depth measurements, the image trajectories are usually very close to straight lines, which is almost sufficient to satisfy the field of view constraints. However, bad estimates of the feature depth in conventional IBVS may lead to trajectories that violate the field of view constraints, thus jeopardizing visual servoing.

Theorem 1. *Consider $n \geq 4$ fixed visual features[4] in the workspace and a pinhole camera that aims at attaining the desired values for the feature coordinates on the image plane, while satisfying the field of view constraints. Under the assumption that all visual features initially lie sufficiently close to their desired values as well as within the field of view of the camera, the proposed image based visual servoing protocol (13) guarantees local practically asymptotic stabilization of the feature errors:*

$$-\underline{M}_i^u \rho_i^u(t) < e_i^u(t) < \bar{M}_i^u \rho_i^u(t),\ i = 1, \ldots, n \tag{15}$$
$$-\underline{M}_i^v \rho_i^v(t) < e_i^v(t) < \bar{M}_i^v \rho_i^v(t),\ i = 1, \ldots, n \tag{16}$$

as well as the boundedness of all closed loop signals for all $t \geq 0$.

Proof. We first define the normalized image feature error vector $\xi = [\xi_1^u, \xi_1^v, \ldots, \xi_n^u, \xi_n^v]^T$. Differentiating with respect to time and substituting (4) and (13), the closed loop dynamical system may be written in compact form as:

$$\dot{\xi} = h(t, \xi) \triangleq \operatorname{diag}(\rho(t))^{-1} \left(-kL\hat{L}^+ E - \operatorname{diag}(\dot{\rho}(t))\, \xi \right) \tag{17}$$

where $\rho(t) \triangleq [\rho_1^u(t), \rho_1^v(t), \ldots, \rho_n^u(t), \rho_n^v(t)]^T$. Let us also define the open set $\Omega_\xi \triangleq \left(-\underline{M}_1^u, \bar{M}_1^u\right) \times \left(-\underline{M}_1^v, \bar{M}_1^v\right) \times \cdots \times \left(-\underline{M}_n^u, \bar{M}_n^u\right) \times \left(-\underline{M}_n^v, \bar{M}_n^v\right)$. In what follows, we proceed in two phases. First, the existence of a maximal solution $\xi(t)$ of (17) over the set Ω_ξ for a time interval $[0,\ \tau_{max})$ is ensured, i.e., $\xi(t) \in \Omega_\xi,\ \forall t \in [0,\ \tau_{max})$. Then, we prove that the proposed control scheme (13) guarantees, for all $t \in [0,\ \tau_{max})$: a) the boundedness of all closed loop signals as well as that b) $\xi(t)$ remains strictly within a compact subset of Ω_ξ, which leads by contradiction to $\tau_{max} = \infty$ and consequently to the satisfaction of (7a)-(7b), thus completing the proof.

Phase A. The set Ω_ξ is nonempty and open. Moreover, (10a)-(10b) lead to $-\underline{M}_i^u < \xi_i^u(0) < \bar{M}_i^u$ and $-\underline{M}_i^v < \xi_i^v(0) < \bar{M}_i^v,\ i = 1, \ldots, n$. Thus, we conclude that $\xi(0) \in \Omega_\xi$. Additionally, $h(t, \xi)$, as defined in (17), is continuous on t and locally Lipschitz on ξ over the set Ω_ξ. Therefore, the hypotheses of Theorem 54 (pp.476) in [31] hold and the existence of a maximal solution $\xi(t)$ of (17) on a time interval $[0,\ \tau_{max})$ such that $\xi(t) \in \Omega_\xi,\ \forall t \in [0,\ \tau_{max})$ is ensured.

Phase B. We have proven in Phase A that $\xi(t) \in \Omega_\xi,\ \forall t \in [0,\ \tau_{max})$ and more specifically that $\xi_i^u(t) \in (-\underline{M}_i^u, \bar{M}_i^u)$ and $\xi_i^v(t) \in (-\underline{M}_i^v, \bar{M}_i^v),\ i = 1, \ldots, n$ for all $t \in [0,\ \tau_{max})$. Thus, the transformed errors $E_i^u,\ E_i^v,\ i = 1, \ldots, n$, as designated in (14), are well defined for all $t \in [0,\ \tau_{max})$. Hence, we may adopt, based on the transformed errors (14), the task function $\varepsilon = \hat{L}^+ E$ [32]. Contrary to [32], where $\hat{L}^+$ is assumed constant, in this work we consider a more generic case where $\hat{L}^+$ is state dependent, with positive and fixed focal length and depth estimates. Thus, the time derivative of the task function becomes:

$$\begin{aligned}
\dot{\varepsilon} &= \frac{d\hat{L}^+}{dt} E + \hat{L}^+ \dot{E} = \frac{d\hat{L}^+}{dt} E + \hat{L}^+ \frac{\partial E}{\partial \xi} \dot{\xi} \\
&= \frac{d\hat{L}^+}{dt} E + \hat{L}^+ \frac{\partial E}{\partial \xi} \left(\frac{\partial \xi}{\partial e} \dot{e} + \frac{\partial \xi}{\partial t} \right) \\
&= \frac{d\hat{L}^+}{dt} E + \hat{L}^+ \frac{\partial E}{\partial \xi} \left(\frac{\partial \xi}{\partial e} LV + \frac{\partial \xi}{\partial t} \right)
\end{aligned} \tag{18}$$

Following [23], we also obtain $\frac{d\hat{L}^+}{dt} E = O(e, t) V$, where $O(e, t)$ is a 6×6 matrix satisfying $O(e, t)|_{e=0} = \mathbf{0}_{6\times 6},\ \forall t \geq 0$. Hence, (18) becomes:

$$\dot{\varepsilon} = \Big(O(e, t) + \hat{L}^+ \big(\frac{\partial E}{\partial \xi} \frac{\partial \xi}{\partial e} \big) L \Big) V + \hat{L}^+ \frac{\partial E}{\partial \xi} \frac{\partial \xi}{\partial t}$$

[4]Although 3 features may suffice to establish locally the full column-rank property of the interaction matrix, we assume at least 4 for increased levels of robustness.

and substituting the control law $V = -k\hat{L}^+ E \triangleq -k\varepsilon$, we get:

$$\dot{\varepsilon} = -k \Big(O(e, t) + \hat{L}^+ \big(\frac{\partial E}{\partial \xi} \frac{\partial \xi}{\partial e} \big) L \Big) \varepsilon + \hat{L}^+ \frac{\partial E}{\partial \xi} \frac{\partial \xi}{\partial t}. \tag{19}$$

Finally, linearizing (19) for $\varepsilon = 0$, we obtain similarly to [23]:

$$\dot{\varepsilon} = -(kA(t) - B(t))\varepsilon + C(t),$$

where:

$$A(t) = \hat{L}^+ \big(\frac{\partial E}{\partial \xi} \frac{\partial \xi}{\partial e} \big) L \Big|_{\varepsilon=0} \tag{20a}$$
$$B(t) = \frac{\partial}{\partial \varepsilon} \left(\hat{L}^+ \frac{\partial E}{\partial \xi} \frac{\partial \xi}{\partial t} \right) \Big|_{\varepsilon=0} \tag{20b}$$
$$C(t) = \hat{L}^+ \frac{\partial E}{\partial \xi} \frac{\partial \xi}{\partial t} \Big|_{\varepsilon=0}. \tag{20c}$$

Notice also that by construction $\frac{\partial E}{\partial \xi} \frac{\partial \xi}{\partial e}$ is a diagonal positive definite matrix. Thus, following similar arguments with [23], we conclude that $A(t) = \hat{L}^+ \big(\frac{\partial E}{\partial \xi} \frac{\partial \xi}{\partial e} \big) L \Big|_{\varepsilon=0}$ is Hurwitz close to the origin for any positive and fixed focal length and depth estimates. Moreover, it can be easily verified that the matrix $B(t)$ and the vector $C(t)$ are bounded for all $t \geq 0$ and vanish as time proceeds owing to the decreasing property of the performance functions. Hence, invoking Lemma 4.5 (pp.193) in [33], we conclude that $\varepsilon(t)$ remains ultimately bounded for a sufficiently high gain value k and all $t \in [0,\ \tau_{max})$ within a neighborhood of $\varepsilon = 0$, i.e., $||\varepsilon(t)|| \leq \bar{\varepsilon}$. Moreover, in a neighborhood of $\varepsilon = 0$, we have $||\varepsilon|| \triangleq ||\hat{L}^+ E|| \neq 0$ if $e \neq 0$ or equivalently if $E \neq 0$, since $\hat{L}^+$ is full row-rank [22]. Hence, there exists $\bar{E} > 0$ such that :

$$||E(t)|| \leq \bar{E},\ \forall t \in [0,\ \tau_{max}). \tag{21}$$

In this way, taking the inverse logarithmic function in (14), we get:

$$\begin{aligned}
&-\underline{M}_i^u < \underline{\xi}_i^u < \xi_i^u(t) < \bar{\xi}_i^u < \bar{M}_i^u \\
&-\underline{M}_i^v < \underline{\xi}_i^v < \xi_i^v(t) < \bar{\xi}_i^v < \bar{M}_i^v
\end{aligned},\ i = 1, \ldots, n \tag{22}$$

for all $t \in [0,\ \tau_{max})$, where:

$$\underline{\xi}_i^u = -\underline{M}_i^u \tfrac{\exp(\bar{E})-1}{\exp(\bar{E})+\frac{\underline{M}_i^u}{\bar{M}_i^u}}, \quad \bar{\xi}_i^v = \bar{M}_i^u \tfrac{\exp(\bar{E})-1}{\exp(\bar{E})+\frac{\underline{M}_i^u}{\bar{M}_i^u}}$$
$$\underline{\xi}_i^v = -\underline{M}_i^v \tfrac{\exp(\bar{E})-1}{\exp(\bar{E})+\frac{\underline{M}_i^v}{\bar{M}_i^v}}, \quad \bar{\xi}_i^v = \bar{M}_i^v \tfrac{\exp(\bar{E})-1}{\exp(\bar{E})+\frac{\underline{M}_i^v}{\bar{M}_i^v}}$$

Finally, it can be easily proven from (14) that the control input (13) remains also bounded for all $t \in [0,\ \tau_{max})$.

Up to this point, what remains to be shown is that τ_{max} can be extended to ∞. Notice by (22) that $\xi(t) \in \Omega'_\xi,\ \forall t \in [0, \tau_{max})$, where the set $\Omega'_\xi = \left[\underline{\xi}_1^u, \bar{\xi}_1^u\right] \times \left[\underline{\xi}_1^v, \bar{\xi}_1^v\right] \times \cdots \times \left[\underline{\xi}_n^u, \bar{\xi}_n^u\right] \times \left[\underline{\xi}_n^v, \bar{\xi}_n^v\right]$ is a nonempty and compact subset of Ω_ξ. Hence, assuming $\tau_{max} < \infty$ and since $\Omega'_\xi \subset \Omega_\xi$, Proposition C.3.6 (pp. 481) in [31] dictates the existence of a time instant $t' \in [0, \tau_{max})$ such that $\xi(t') \notin \Omega'_\xi$, which is a clear contradiction. Therefore, $\tau_{max} = \infty$. As a result, all closed loop signals remain bounded and moreover $\xi(t) \in \Omega'_\xi \subset \Omega_\xi,\ \forall t \geq 0$. Finally, from (22) we conclude the satisfaction of (7a)-(7b) for all $t \geq 0$ and consequently prescribed transient and steady state performance without violating the field of view constraints, which completes the proof. □

Remark 5. *From the aforementioned proof, it can be deduced that the proposed image based visual servoing scheme achieves its goals (i.e., prescribed performance and field of view constraints) without residing on the need of rendering $\bar{E}$ arbitrarily small (see (21)), by adopting an extreme value for the control gain k. More specifically, notice that (22) and consequently* (7a)-(7b)*, which encapsulate the prescribed performance notion and the field of view constraints, hold no matter how large the finite bound $\bar{E}$ is. Thus, contrary*

to what is the common practice in the related literature (i.e., the control gains are tuned towards satisfying a desired performance, nonetheless without any a priori guarantees), the actual performance of the proposed IBVS scheme is solely determined by the performance functions $\underline{M}_i^u \underline{\rho}_i^u(t)$, $\bar{M}_i^u \bar{\rho}_i^u(t)$, $\underline{M}_i^v \underline{\rho}_i^v(t)$, $\bar{M}_i^v \bar{\rho}_i^v(t)$, $i = 1, \ldots, n$. Hence, the selection of the control gain k is significantly simplified to adopting those values that lead to reasonable control effort.

Remark 6. *Contrary to the existing works in the related literature, where the depth and camera calibration errors influence severely the performance of the visual servoing, in the proposed work the achieved performance is a priori determined by the selection of $\underline{M}_i^u \underline{\rho}_i^u(t)$, $\bar{M}_i^u \bar{\rho}_i^u(t)$, $\underline{M}_i^v \underline{\rho}_i^v(t)$, $\bar{M}_i^v \bar{\rho}_i^v(t)$, $i = 1, \ldots, n$. However, it should be stressed that the aforementioned errors affect the region of attraction of the closed loop system around the origin, thus leading to local stability results. Studying the effect of camera calibration and depth distribution errors to obtain the size of the robust initialization domain goes beyond the scope of this work and is left open for future research.*

IV. Experimental Results

To validate the theoretical findings and verify the efficiency of the proposed IBVS scheme, a comparative experimental study with a conventional IBVS controller [1] was conducted, employing an eye-in-hand robotic system.

A. System Components and Parameters

The robotic system used in this work is a 7 DoFs robotic manipulator Mitsubishi PA-10, equipped with a calibrated perspective USB camera (Sony PlayStation Eye), with 640×480 pixels at 30 frames per second and focal length $\lambda = 538$ pixels, rigidly attached on its end-effector. The software architecture is based on the Robot Operating System (ROS) in Ubuntu Linux and the IBVS algorithms were developed in C++ and Python. The target is fixed and consists of four markers (forming a square of 15 cm edge), the center of which denotes an image feature that is detected in real time using the ROS implementation of the Computer Vision ArToolkit library. The desired feature coordinates $s^* = \begin{bmatrix} -240 & 55 & -251 & 45 \\ -128 & -119 & 169 & 172 \end{bmatrix}$ were extracted by a still image captured at the desired pose of the camera heading towards the features. The depth in the desired position was measured at $z_i^* = 0.36\text{m}$, $i = 1, \ldots, 4$. In addition, the gains of the proposed and the conventional IBVS schemes were selected as 0.3 and 0.018, respectively. Furthermore, the parameters $\underline{M}_i^u$, $\bar{M}_i^u$, $\underline{M}_i^v$, $\bar{M}_i^v$, $i = 1, \ldots, 4$ are chosen such that all features are retained within the camera field of view for all time. In particular, the following upper and lower bounds of the image plane: $u_{\min} = -319$, $u_{\max} = 319$, $v_{\min} = -239$, $v_{\max} = 239$ were adopted in (9a) and (9b) to extract the values of the parameters $\underline{M}_i^u$, $\bar{M}_i^u$, $\underline{M}_i^v$, $\bar{M}_i^v$, $i = 1, \ldots, 4$. Moreover, the maximum allowable steady state error was set equal to $\rho_\infty = 10$ pixels. Thus, each feature will be ultimately confined within a square of 20 pixels edge, centered at the desired position on the image plane. Finally, the decreasing rate l was chosen equal to $l = 0.2$ to enforce an exponential convergence dictated by $\exp(-0.2t)$.

B. Comparative Study

The robustness and guaranteed convergence properties of the proposed IBVS scheme as well as its efficiency in handling the camera field of view constraints are demonstrated via a comparative experimental study with a conventional IBVS scheme [1]. The initial camera configuration in all experiments was [-0.55,-0.62,1.12] m with respect to the centroid of the features, pointing towards them. Consequently, the initial feature coordinates were extracted as $s(0) = \begin{bmatrix} -149 & 49 & -160 & 68 \\ -109 & -115 & 79 & 75 \end{bmatrix}$. It should be noticed that the aforementioned initial configuration can be considered as rather challenging for IBVS schemes, owing to the large rotation about the x axis of the camera frame that is needed to converge to the desired configuration. Two cases with: i) accurately measured depth and ii) fixed depth values were considered. For each case, the comparison was performed via two experiments. The proposed IBVS scheme was employed in the first experiment, and a conventional IBVS scheme was used in the latter. In both experimental studies, comparisons are made to show the efficacy and superior performance of the proposed scheme in handling field of view constraints versus the conventional IBVS scheme. Finally, a HD video demonstrating the experiments can be found at the following url:

https://youtu.be/PZNJropsGIo

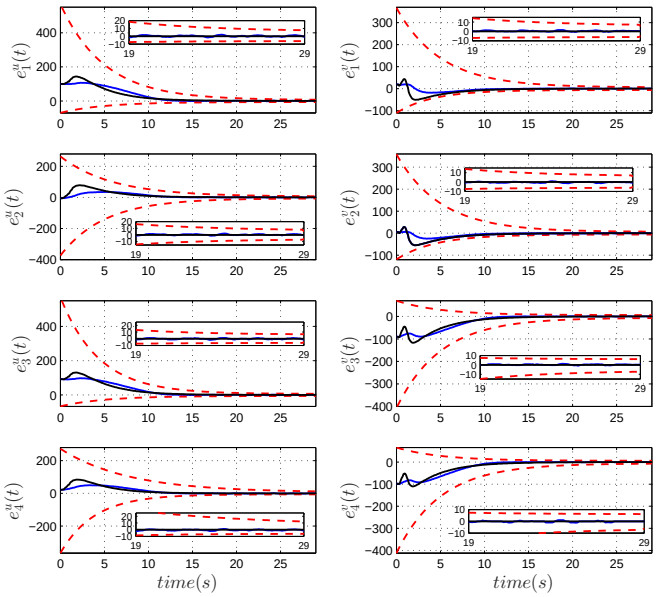

Fig. 2: **Case I:** The evolution of the feature coordinate errors along with the corresponding imposed performance bounds employing the **proposed** (blue) and the **conventional** (black) IBVS schemes.

Case I: Accurate depth measurement

In this study, the depth measurement for each image feature was available in both the proposed and the conventional IBVS algorithms via the visual tracking system. The results are presented in Fig.2, where the evolution of the image feature errors employing the proposed and the conventional IBVS schemes are presented. As it was expected, the feature coordinate errors in the scenario with the proposed IBVS scheme were retained within the corresponding performance envelopes and consequently the features were constantly kept within the camera field of view. Similarly, notice for the conventional IBVS scheme that the image features were kept within the camera field of view as well (although they reached very close to the image boundaries), while satisfactory convergence was also achieved. However, it should be noted that the illustrated results for the conventional IBVS scheme were attained through a trial and error selection procedure of the control gains in order to: i) achieve similar convergence properties with the proposed scheme and ii) result in reasonable control effort. On the contrary, the control gain of the proposed scheme was selected only to meet the joint velocity limits

of the manipulator, which were sufficient to achieve the imposed transient response specifications presented in the previous subsection.

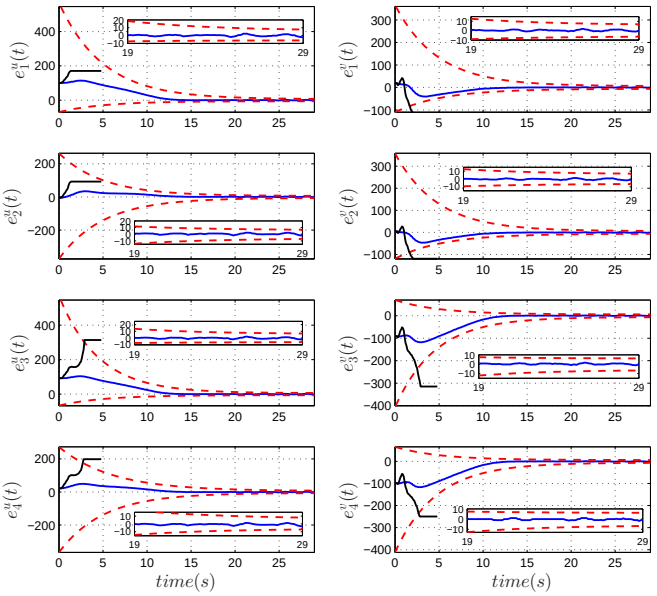

Fig. 3: **Case II:** The evolution of the feature coordinate errors along with the corresponding imposed performance bounds employing the **proposed** (blue) and the **conventional** (black) IBVS schemes.

Case II: Fixed depth estimate

In this case study, the same challenging initial configuration was considered without however employing accurate depth measurements in the interaction matrix. Instead, the following fixed depth values were adopted $z_i^* = 0.36,\ i = 1,\ldots,4$ that were extracted at the desired configuration (i.e., the distance of the features to the camera plane when the camera is positioned at the desired pose with respect to the features). The results are illustrated in Fig.3, where the evolution of the image feature errors employing the proposed and the conventional IBVS schemes are presented. As it was expected from the theoretical findings of this work, even in the case of incorrect depth values, the feature coordinate errors were retained in the corresponding performance envelopes and consequently the features were constrained within the camera field of view. Moreover, it can be seen from Fig.3 that the convergence properties of the proposed IBVS scheme remained unaltered. On the contrary, noticing the evolution of the image feature errors for the conventional IBVS, we conclude that the particular experiment failed as the features escaped the image boundaries. Finally, it should be noted that the control gains were kept unaltered in both Cases I and II, thus revealing that the control gain selection in the proposed IBVS scheme has been significantly simplified since it is decoupled by both the closed loop transient and steady state response as well as the satisfaction of the camera field of view constraints.

V. Simulation Results

We conducted an extensive comparative simulation study to emphasize on the benefits of our approach and demonstrate its high levels of robustness. More specifically, we considered the camera model that we used for the experiments. Four features were also located in the y-z plane at the positions $P_1 = [0, -0.2, 0.15]^T$ m, $P_2 = [0, 0.2, 0.15]^T$ m, $P_3 = [0, -0.2, -0.15]^T$ m and $P_4 = [0, 0.2, -0.15]^T$ m. The desired camera pose was selected on the x-axis as $P_d = [0.6725, 0, 0]^T$ m heading towards the features with orientation $R_d = rot_y(-90^o)rot_z(90^o)$. Hence, the desired feature coordinates on the image plane were calculated as $s_1^d = [-160, -120]^T$ pixels, $s_2^d = [160, -120]^T$ pixels, $s_3^d = [-160, 120]^T$ pixels, $s_4^d = [160, 120]^T$ pixels. Then, 200 initial camera configurations were randomly extracted (following a uniform distribution in spherical coordinates from the set $\rho \in [1.3, 3.2]$ m, $\theta \in [45^o, 135^o]$, $\phi \in [-45^o, 45^o]$), with the features lying initially within the camera field of view, as shown in Fig. 4. For each initial camera configuration, we simulated the camera kinematics for 10 sec, under both the conventional IBVS control scheme [1] and the proposed one. In particular, the estimate of the interaction matrix in both cases involved a 5% camera calibration error in the focal length (a rather reasonable level of accuracy for a chessboard calibration procedure) and the desired feature depth $z_d = 0.6725$ m (i.e., no actual depth measurements were employed). Moreover, the gain of the conventional IBVS scheme was set $k = 1$, whereas for the proposed scheme we adopted $k = 500$. Notice that the difference in the order of magnitude comes from the fact that in the conventional IBVS scheme the errors are defined in pixels, while in the proposed scheme the pixel errors are first normalized with respect to the performance functions and then modulated through the logarithmic function to output the transformed errors E_i^u and E_i^v. Furthermore, we selected $\rho_{\inf} = 3$ and exponential rate $l = 1$ for all simulations. Finally, based on the camera field of view, we chose $u_{\min} = -320$, $u_{\max} = 320$, $v_{\min} = -240$, $v_{\max} = 240$.

From the 200 initial configurations the conventional IBVS controller managed to achieve convergence and retain the features within the camera field of view in only 10 cases. It should be noticed that the same controller with perfect knowledge in the interaction matrix (i.e., accurate focal length and accurate depth measurements) succeeded both objectives in all initial camera configurations. On the other hand, the proposed scheme under the aforementioned model uncertainty succeeded in 122 cases to establish the predefined transient and steady state performance specifications, which reveals that it is more robust than the conventional IBVS scheme especially in satisfying the field of view constraints which are critical for the operation of visual servoing. Notice that for the 78 cases that it failed apparently the Hurwitz property for (20a) was not satisfied. However, this was the case for the conventional IBVS scheme as well. Therefore, we may fairly say that owing to model uncertainties the domain of attraction (if the field of view constraints are also considered in the evaluation) shrinks less in the proposed scheme than in the conventional IBVS.

VI. Future Directions

Studying the effect of camera calibration and depth distribution errors to obtain the magnitude of the robust initialization domain deserves a thorough investigation of the structural properties of the interaction matrix and is left open for future research. In the same spirit, considering non-holonomic constraints as well as dynamic uncertainty on the camera motion model is a promising direction that would increase the applicability of the proposed IBVS scheme. Finally, the method proposed in [34] that allows certain visual features to leave from the field of view temporarily, based on the concept of weighted features, could be integrated with the proposed approach in order to handle abrupt motions of the target that would drive certain features outside the camera field of view.

References

[1] F. Chaumette and S. Hutchinson, "Visual servo control. i. basic approaches," *IEEE Robotics and Automation Magazine*, vol. 13, no. 4, pp. 82–90, 2006.

[2] ——, "Visual servo control, part ii: Advanced approaches," *IEEE Robotics and Automation Magazine*, vol. 14, no. 1, pp. 109–118, 2007.

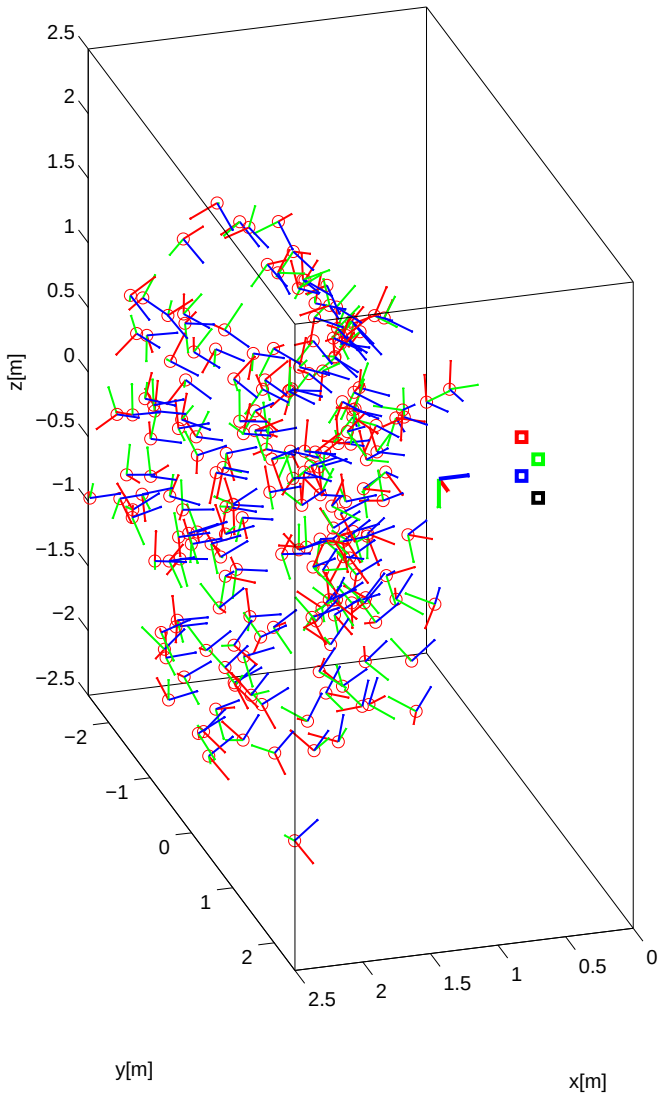

Fig. 4: The initial camera poses. The features are depicted with colored squares and the initial camera positions with red circles. The orientation of the camera is given by a frame with x(red), y(green) and z(blue) axis. The desired camera pose is given with thick colored axis in front of the features.

[3] F. Chaumette, "Potential problems of stability and convergence in image-based and position-based visual servoing," in *The confluence of vision and control*. Springer London, 1998, vol. 237, pp. 66–78.

[4] P. Corke and S. Hutchinson, "A new partitioned approach to image-based visual servo control," *IEEE Transactions on Robotics and Automation*, vol. 17, no. 4, pp. 507–515, 2001.

[5] G. Chesi, K. Hashimoto, D. Prattichizzo, and A. Vicino, "Keeping features in the field of view in eye-in-hand visual servoing: A switching approach," *IEEE Transactions on Robotics*, vol. 20, no. 5, pp. 908–913, 2004.

[6] N. Gans and S. Hutchinson, "Stable visual servoing through hybrid switched-system control," *IEEE Transactions on Robotics*, vol. 23, no. 3, pp. 530–540, 2007.

[7] O. Kermorgant and F. Chaumette, "Combining ibvs and pbvs to ensure the visibility constraint," *IEEE International Conference on Intelligent Robots and Systems*, pp. 2849–2854, 2011.

[8] X. Li and C. C. Cheah, "Global task-space adaptive control of robot," *Automatica*, vol. 49, no. 1, pp. 58–69, 2013.

[9] N. Cowan, J. Weingarten, and D. Koditschek, "Visual servoing via navigation functions," *IEEE Transactions on Robotics and Automation*, vol. 18, no. 4, pp. 521–533, 2002.

[10] Y. Mezouar and F. Chaumette, "Path planning for robust image-based control," *IEEE Transactions on Robotics and Automation*, vol. 18, no. 4, pp. 534–549, 2002.

[11] F. Schramm, F. Geffard, G. Morel, and A. Micaelli, "Calibration free image point path planning simultaneously ensuring visibility and controlling camera path," *Proceedings - IEEE International Conference on Robotics and Automation*, pp. 2074–2079, 2007.

[12] G. Chesi and Y. Hung, "Global path-planning for constrained and optimal visual servoing," *IEEE Transactions on Robotics*, vol. 23, no. 5, pp. 1050–1060, 2007.

[13] G. Chesi, "Visual servoing path planning via homogeneous forms and lmi optimizations," *IEEE Transactions on Robotics*, vol. 25, no. 2, pp. 281–291, 2009.

[14] A. Hafez, A. Nelakanti, and C. Jawahar, "Path planning for visual servoing and navigation using convex optimization," *International Journal of Robotics and Automation*, vol. 30, no. 3, pp. 299–307, 2015.

[15] E. C. G. Allibert and Y. Toure, "Real-time visual predictive controller for image-based trajectory tracking of a mobile robot," *Proceedings of the 17th IFAC World Congress*, pp. 11 244–11 249, 2008.

[16] G. Allibert, E. Courtial, and F. Chaumette, "Predictive control for constrained image-based visual servoing," *IEEE Transactions on Robotics*, vol. 26, no. 5, pp. 933–939, 2010.

[17] A. Mcfadyen, P. Corke, and L. Mejias, "Visual predictive control of spiral motion," *IEEE Transactions on Robotics*, vol. 30, no. 6, pp. 1441–1454, 2014.

[18] Y.-H. Liu, H. Wang, C. Wang, and K. K. Lam, "Uncalibrated visual servoing of robots using a depth-independent interaction matrix," *IEEE Transactions on Robotics*, vol. 22, no. 4, pp. 804–817, 2006.

[19] H. Wang, Y.-H. Liu, and D. Zhou, "Dynamic visual tracking for manipulators using an uncalibrated fixed camera," *IEEE Transactions on Robotics*, vol. 23, no. 3, pp. 610–617, 2007.

[20] ——, "Adaptive visual servoing using point and line features with an uncalibrated eye-in-hand camera," *IEEE Transactions on Robotics*, vol. 24, no. 4, pp. 843–857, 2008.

[21] H. Wang, "Adaptive visual tracking for robotic systems without image-space velocity measurement," *Automatica*, vol. 55, pp. 294–301, 2015.

[22] E. Malis and F. Chaumette, "Theoretical improvements in the stability analysis of a new class of model-free visual servoing methods," *IEEE Transactions on Robotics and Automation*, vol. 18, no. 2, pp. 176–186, 2002.

[23] E. Malis and P. Rives, "Robustness of image-based visual servoing with respect to depth distribution errors," in *IEEE International Conference on Robotics and Automation (ICRA)*, 2003, pp. 1056–1061.

[24] X. Zhong, X. Zhong, and X. Peng, "Robots visual servo control with features constraint employing kalman-neural-network filtering scheme," *Neurocomputing*, vol. 151, no. P1, pp. 268–277, 2015.

[25] Z. Miljkovi, M. Miti, M. Lazarevi, and B. Babi, "Neural network reinforcement learning for visual control of robot manipulators," *Expert Systems with Applications*, vol. 40, no. 5, pp. 1721–1736, 2013.

[26] G. Morel, P. Zanne, and F. Plestan, "Robust visual servoing: Bounding the task function tracking errors," *IEEE Transactions on Control Systems Technology*, vol. 13, no. 6, pp. 998–1009, 2005.

[27] F. Schramm and G. Morel, "Ensuring visibility in calibration-free path planning for image-based visual servoing," *IEEE Transactions on Robotics*, vol. 22, no. 4, pp. 848–854, 2006.

[28] S. Heshmati-Alamdari, C. Bechlioulis, M. Liarokapis, and K. Kyriakopoulos, "Prescribed performance image based visual servoing under field of view constraints," *IEEE International Conference on Intelligent Robots and Systems*, pp. 2721–2726, 2014.

[29] C. P. Bechlioulis and G. A. Rovithakis, "Prescribed performance adaptive control for multi-input multi-output affine in the control nonlinear systems," *IEEE Transactions on Automatic Control*, vol. 55, no. 5, pp. 1220–1226, 2010.

[30] ——, "A low-complexity global approximation-free control scheme with prescribed performance for unknown pure feedback systems," *Automatica*, vol. 50, no. 4, pp. 1217–1226, 2014.

[31] E. D. Sontag, *Mathematical Control Theory*. London, U.K.: Springer, 1998.

[32] B. Espiau, F. Chaumette, and P. Rives, "A new approach to visual servoing in robotics," *IEEE Transactions on Robotics and Automation*, vol. 8, no. 3, pp. 313–326, 1992.

[33] H. K. Khalil, *Nonlinear Systems*, 1st ed. Macmillan, 1992.

[34] N. García-Aracil, E. Malis, R. Aracil-Santonja, and C. Pérez-Vidal, "Continuous visual servoing despite the changes of visibility in image features," *IEEE Transactions on Robotics*, vol. 21, no. 6, pp. 1214–1220, 2005.